ELSEVIER

Chemical Engineering Journal 72 (1999) 125–138

Chemical Engineering Journal

Determination of local energy dissipation rates in impinging jets by a chemical reaction method

Eric Schaer*, Pierrette Guichardon, Laurent Falk, Edouard Plasari

Laboratoire des Sciences du Génie Chimique, CNRS - ENSIC, 1 rue Grandville, BP 451, 54001 Nancy Cedex, France

Received 22 March 1998; received in revised form 27 October 1998; accepted 3 November 1998

Abstract

To carry out controlled precipitation on a practical scale, the use of a two impinging jets mixer is explored in terms of its ability to deliver rapid micromixing. A system of parallel competing reactions developed by Villermaux and co-workers is used to characterise the micromixing level in the device as a function of feed flow rate and of its position in the reactor. The characteristic time for micromixing decreases with the feed flow rate and reaches values as small as 4 ms. Powers dissipated in the device are deduced from the experiments using a simple micromixing model and correlate well with those calculated using computational fluid dynamics (Phoenics). Finally, the energy dissipation rate in impinging jets is compared with the local energy dissipation rate of the impeller. Some rules of thumb for scale up are given.

1. Introduction

Sparingly soluble systems are often produced by a precipitation process. In industrial practice, precipitation typically consists in mixing of two liquid streams, to create supersaturation, which then induces nucleation and particle growth. The precipitation processes are frequently followed by solid–liquid separation processes, to obtain a dry product. Most of the time, the final product has to fulfil specific qualities as crystal size, morphology, composition or purity.

When the time scale of the precipitation kinetics is much longer than the time scale of mixing, the mixing processes of the two liquid streams are terminated prior to the reaction. In this case, the final product characteristics mainly depend on physico-chemical parameters, but not on mixing conditions. However, precipitation processes are often controlled by the mixing process: indeed, when precipitation kinetics are faster or of the same order of the mixing process, nucleation begins before an homogeneous supersaturation level is achieved in the reactor. The inhomogeneous field of supersaturation causes then different driving forces for nucleation and particle growth, which then drastically affects the final product properties.

The role of macro- and micromixing in precipitation has been identified by several researchers. Various mixing models [1–3] have been proposed and computed for continuous and semi-batch stirred tank precipitators. Design factors, such as feed addition mode, feed rate, feed location, feed concentration, stirring speed, and stirrer type have been shown to affect the resulting average particle size [4–6]. It becomes quite clear, from these studies, that the localised supersaturation level in stirred tank precipitators is one of the most important factor that controls the final Particle Size Distribution (PSD) by influencing the nucleation and growth rates of particles.

Therefore, to minimise mixing effects, we have developed a new mixing device driving to very short contact and micromixing times. Among several methods leading to a reduction of mixing time, we have chosen to use a system that reduces the initial contact scale between the reactants and that dissipates power in a volume smaller than that of the whole reactor. Two impinging jets mixer is one of such a technique, in which two liquid streams in a form of narrow, coaxial and high velocity jets impinge each other inside a small volume.

The various utilizations of impinging jets have been reported by Tamir and Kitron [7]. Impinging jets were, until now, mainly used to increase the contact areas between two fluids (to improve heat or mass transfer in gas–liquid–solid applications), or to produce a spray of fuel droplets that can be combusted easily.

The use of impinging jets in the fields of precipitation or crystallisation is relatively recent. To our knowledge, Midler

*Corresponding author. Tel.: +33-3-83-17-5304; fax: +33-3-83-17-5319; e-mail: schaer@ensic.u-nancy.fr

1385-8947/99/$ – see front matter
PII: S1385-8947(98)00152-1

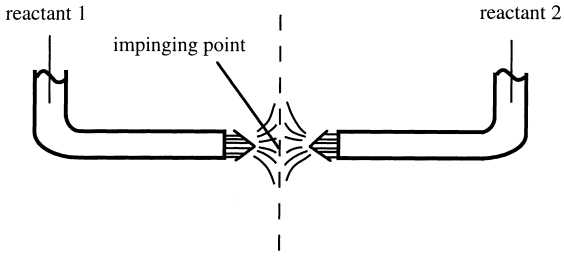

Fig. 1. Impinging jets.

et al. [8] in 1989 were first to apply impinging jets to the precipitation of pharmaceutical products. They show that impinging jets achieve good micromixing and uniform supersaturation level in the reactor which leads to a highly reproducible final product. Liu et al. [9] used the same system for the production of steroids. They came to the same conclusions, and estimated micromixing times achieved by impinging jets from the calculation of locally dissipated energies. Finally, Mahajan and Kirwan [10] applied impinging jets to the precipitation of Lovastatin, and used the two-steps Bourne [11] reaction scheme to characterise micromixing in the impinging jets. In impact conditions of the two jets, they show that the distance between the tube outlets had little influence on the product characteristics and that micromixing affected the PSD of the precipitated product only when the micromixing time was comparable to or larger than the nucleation induction time.

The aim of this study is to characterise the mixing intensity induced by the impinging jets, and more precisely, to quantify the local energy dissipation rates in the device, at the impingement point (see Fig. 1), for different jets location in the reactor and for different total feed flow rates. Furthermore, some designing rules will be proposed.

2. Impinging jets

An impinging jets mixer was used in the present study and is shown in Fig. 1. Two small diameter (1 mm diameter), high velocity jets, brought into alignment with each other, impinge head-on. The mixing device was systematically operated in a submerged mode in a 10 l capacity stirred tank reactor, designed according to Holland and Chapman [16]. The reactor was equipped with four baffles placed at 90° intervals and a six bladed Rushton turbine. Impinging jets plane is tangentially located to the stirrer, at 46 mm of the wall, as can be seen in Fig. 2. The jet device is adjustable in height and in azimuthal orientation. The distance between the two feeding inlet has been maintained constant and equal to 10 mm for all experiments. Jets feeds are supplied by two peristaltic pumps, at identical flow rates, in the range from 0 to 5×10^{-3} l s^{-1}.

Different positions of impinging jets have been tested: in the discharge stream of the impeller (position 0), in the plane above (position 1) or in the plane below (position 2). These three injection points are presented in Fig. 3. The tank reactor was operated in semi-batch mode. The vessel was initially filled up to 67% of its capacity and fed at identical flow rates by impinging jets up to H = T.

Impinging jets achieve macro- and micromixing between the two inlet fluids. The macromixing, characterising the contact efficiency between the two streams, will not be quantified in this paper. The purpose of this study is to apply a chemical reaction method, developed by Villermaux and co-workers [12,13] to measure the micromixing level induced by impinging jets. Micromixing times and local energy dissipation rates will then be deduced from the experiments, using a micromixing model, i.e. the incorporation model [20].

3. The chemical test reaction

3.1. Principle

The characterisation method of micromixing is based on the competition of two chemical reactions. The first one is an instantaneous acid–base neutralisation, whereas the

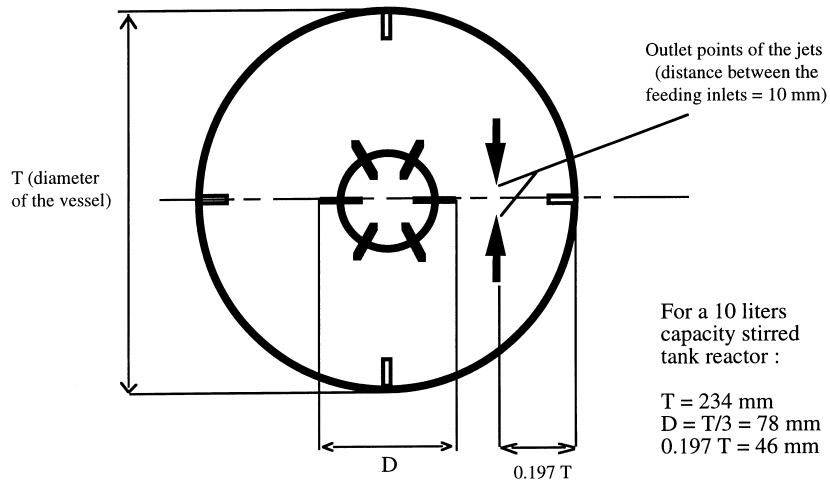

Fig. 2. Impinging jets locations – Tank reactor seen from the top.

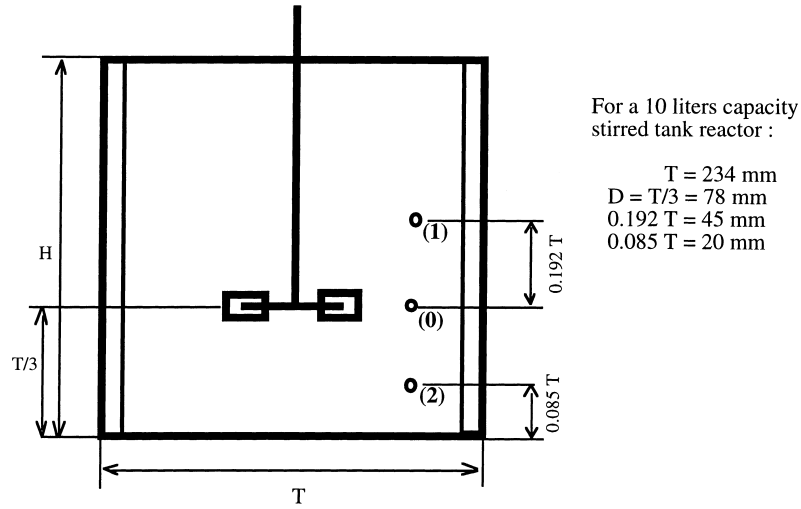

Fig. 3. Impinging jets locations – Front view of the tank reactor.

second one is an oxidation reaction, which rate is only fast, but on the same order of magnitude as that of the micromixing process.

$$H_2BO_3^- + H^+ \rightarrow H_3BO_3 \quad \text{(i)}$$

$$5I^- + IO_3^- + 6H^+ \leftrightarrow 3I_2 + 3H_2O \quad \text{(ii)}$$

The formed iodine further reacts instantaneously with iodide according to the reaction (iii) to form triiodide, whose concentration is easily measured by spectrophotometry.

$$I_2 + I^- \leftrightarrow I_3^- \quad \text{(iii)}$$

This last reaction is characterised by an equilibrium constant [14]

$$K = \frac{C_{I_3^-}}{C_{I_2} C_{I^-}} \quad (1)$$

The test consists in adding sulphuric acid to an excess of iodide, iodate and borate. Under perfect micromixing conditions, acid is totally and instantaneously consumed by the neutralization reaction (i), which is infinitely faster than reaction (ii), as it is in stoichiometric defect with respect to borate ions. In this conditions, no iodine is formed. On the contrary, when the characteristic dissipation time of acid aggregates (micromixing time t_m) is of the same order or larger than the characteristic reaction time (t_r) of the redox reaction (ii), these aggregates involve a local excess of acid which, after complete consumption of borate ions, can react with surrounding iodide and iodate ions to yield iodine.

The selectivity in iodine formation is therefore a measure of the segregation state of the fluid, which can be characterised by a segregation index X_s.

3.2. Determination of the segregation index

The segregation index is defined as the relative amount of acid which is consumed to yield iodine [23].

Let us first consider reactions (i) and (ii). Starting from a mixture containing, $n^0_{H_2BO_3^-}$, $n^0_{I^-}$ (in excess) and $n^0_{IO_3^-}$ moles of borate, iodide and iodate ions, a small amount $n^0_{H^+}$ of sulphuric acid is added to that mixture. After total consumption of acid, the yield of the second reaction under imperfect mixing conditions is

$$Y = 2\frac{n_{I_2}}{n^0_{H^+}} \quad (2)$$

where n_{I_2} is the amount of iodine formed by the oxidation reaction (ii).

If mixing is much faster than reaction (ii), acid is consumed only by the instantaneous reaction (i), and $n_{I_2} = 0$. In this case

$$Y_{PM} = 0 \,(\text{PM for Perfect Mixing conditions}) \quad (3)$$

Conversely, if mixing process is infinitely slow, both reactions (i) and (ii) may be considered as instantaneous with respect to H^+. The selectivity between (i) and (ii) is controlled only by the ratio of the concentrations of $H_2BO_3^-$ and IO_3^-, which react quasi-instantaneously with H^+. Taking into account the stoichiometry, this selectivity is written

$$\frac{X_2}{X_1} = \frac{6n^0_{IO_3^-}}{n^0_{H_2BO_3^-}} \quad (4)$$

where X_1 and X_2 are the respective extents of reaction (i) and (ii).

The yield of the second reaction can then be written as

$$Y_{TS} = \frac{X_2}{X_1 + X_2} = \frac{6n^0_{IO_3^-}}{6n^0_{IO_3^-} + n^0_{H_2BO_3^-}}$$

(TS for Total Segregation conditions.) (5)

According to the definition given above, the segregation index is

$$X_s = \frac{Y}{Y_{TS}} = \frac{n_{I_2}}{n^0_{H+}}\left(2 + \frac{n^0_{H_2BO_3^-}}{3n^0_{IO_3^-}}\right) \quad (6)$$

Actually, taking into account equilibrium (iii), n_{I_2} should be replaced by $(n_{I_2} + n_{I_3^-})$. By spectrophotometry, the measured quantity is $n_{I_3^-}$ but $(n_{I_2} + n_{I_3^-})$ can easily be calculated from the equilibrium constant of reaction (iii).

Finally

$$X_s = \frac{n_{I_2} + n_{I_3^-}}{n^0_{H+}}\left(2 + \frac{n^0_{H_2BO_3^-}}{3n^0_{IO_3^-}}\right) \quad (7)$$

For perfect micromixing, X_s is equal to zero, and in a totally segregated medium, X_s is equal to one.

A micromixedness ratio α can also be defined as the fraction of perfectly micromixed volume of fluid divided by the fraction of volume of fluid remaining segregated

$$\alpha = \frac{1 - X_s}{X_s} \quad (8)$$

The interest of α is that it is closely related to the ratio of two characteristic times: the chemical reaction time t_r of reaction (ii), and a physical micromixing time t_m [15]. For identical initial concentrations of reactants (t_r constant), the variations of α translate faithfully that of t_m. By comparing the micromixedness ratio values, it is then possible to select the device with the higher mixing performance.

4. Experimental procedure

The chemical test reaction may be applied in different ways:

Procedure 1: The reactor is initially filled to 67% of its capacity with the iodide–iodate–borate solution. Impinging jets are fed at identical flow rates with the same solution that the one already placed in the reactor. Sulphuric acid is injected between the two jets at the impingement point with a syringe needle in order to minimise jets flow perturbations, as shown in Fig. 4. If no large scale concentration gradients are present, which will be verified by studying the influence of acid feed time (see Section 4.2), the mixing is only controlled by micromixing. This procedure allows the measurement of micromixing times and a quantification of local energy dissipation rates.

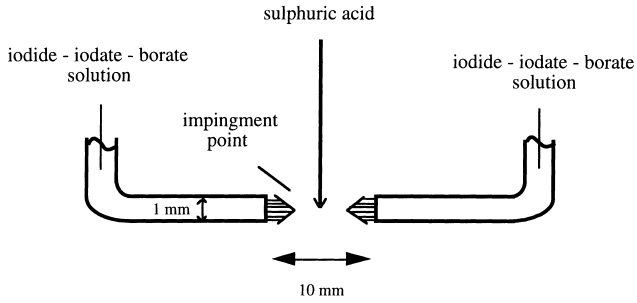

Fig. 4. Feeding of the reactants, procedure 1.

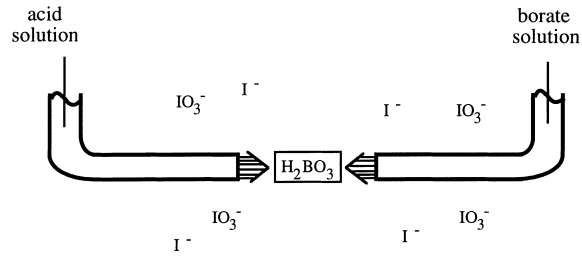

Fig. 5. Feeding of the reactants, procedure 2, not tested (acid solution is fed with one jet and borate solution with the other one in a iodide–iodate ions medium).

Procedure 2: The acid solution is fed with one jet and borate solution with the other one in a iodide–iodate ions medium (Fig. 5). In perfect macro- and micromixing conditions (perfect contact of the two jets) acid reacts with borate ions, and no iodine is formed. Iodine concentration is then a measure of the bad contact efficiency (macro and micro levels) of the two jets. Fig. 6 presents a slightly different procedure, which can also be considered as a contact characterisation method. In this case, iodine concentration is a measure of the quality of macro- and micromixing conditions.

However in procedure 2 it is not possible, from rough experimental data, to separate the respective effects of macro- and micromixing. For this purpose a complete turbulent flow model including micromixing phenomena has to be used. This paper deals with the results obtained with procedure 1, for which a simple micromixing model may be sufficient for data analysis.

4.1. Operating conditions

The concentrations used in the experiments were 9.09×10^{-2} M for borate ions, 1.17×10^{-2} M for iodide ions and 2.33×10^{-2} M for iodate ions.

The tank was then first filled with 6660 ml of the borate, iodide and iodate ions solution. Once the required stirring speed was achieved, the jets were fed, at identical flow rates, with the borate–iodide–iodate solution of the same initial composition as in the tank. Then, a small volume (8.5 ml) of 4 M sulphuric acid was slowly injected, at the impingement point.

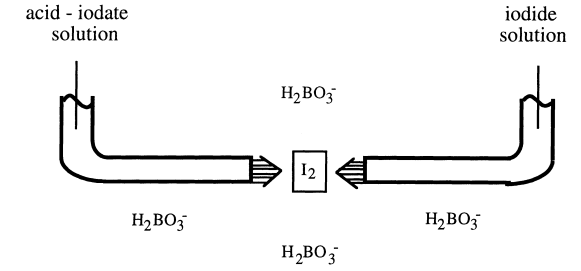

Fig. 6. Feeding of the reactants, procedure 2, not tested (acid–iodate solution is fed with one jet and iodide solution with the other one in a borate ions medium).

After acid injection and consumption, the quantity of iodine produced during the test was deduced from the triiodide concentration, measured by spectrophotometry. The analysis was performed at 353 nm, and the triiodide concentration was deduced from Beer–Lambert's law

$$C_{I_3^-} = \frac{D_{353}}{\varepsilon_{I_3^-}\, d} \tag{9}$$

The equivalent iodine concentration was determined from the mass balance on iodine

$$(C_{I_2})_{tot} = \frac{D_{353}}{\varepsilon_{I_3^-}\, d}\left(1 + \frac{1}{KC_{I^-}}\right) \tag{10}$$

As the test reaction was performed in large excess of iodide with respect to H^+ ions, we may reasonably assume that the final iodide concentration is nearly equal to the initial one, $C_{I^-} = C^0_{I^-}$

The segregation index X_s and the micromixedness ratio α have been determined from Eqs. (7) and (8).

4.2. Influence of acid feed time

In order to characterise conditions where micromixing is free from macromixing influence, the acid feed rate must be as low as possible. Indeed, it is well known [13,17,22] that the acid feed time (or the acid feed flow rate, since a constant quantity of acid is injected) has an influence on the segregation index.

For rapid acid injection conditions, the acid plume is not well dispersed in the tank and macroscopic concentration gradients may influence the results, yielding high values of the segregation index. In the opposite situation, when acid injection is infinitely low, macromixing effects are eliminated and the results given by chemical test reactions are only micromixing relevant. X_s decreases then when the feed time increases, to reach a constant value. A critical injection time t_c is defined as the minimum time beyond which the segregation index value remains constant. Micromixing measurements are to be realised with injection times higher than t_c, which has to be determined for each procedure (reactants concentrations) and for the worst micromixing operating conditions.

In the worst mixing conditions (stirring speed of 190 rpm, total feed flow rate of the iodide–iodate–borate solution varying from 0 to $1 \times 10^{-2}\,l\,s^{-1}$) we checked that the measured critical injection time t_c was less than 150 s. Therefore, to keep a safety margin, all experiments have been performed with an acid feed time of 200 s.

5. Results: influence of feed flow rate and feed location

Various parameters, such as feed time, feed flow rate, stirring speed or feed location have been studied.

In Fig. 7 are presented the variations of the micromixedness ratio α against the feed flow rate in the impinging jets, for various stirring speeds. The flow rate indicated here corresponds to the total feed flow rate equal to two times the individual jet flow rate. The experimental setup (position of the impinging jets device) has not been modified for null flow rate conditions.

Besides the fact that the micromixedness ratio increases, as expected, with the stirring speed, one can observe that α varies with the feed flow rate. More precisely at constant stirring speed, at low feed flow rates ($Q_t < 2 \times 10^{-3}\,l\,s^{-1}$, or jet velocity smaller than $1\,m\,s^{-1}$), the impinging jets have almost no influence on micromixing which is only controlled by the flow generated by the impeller. At intermediate feed flow rates ($2 \times 10^{-3}\,l\,s^{-1} < Q_t < 5 \times 10^{-3}\,l\,s^{-1}$, which corresponds to jets velocity between 1 and 3 m s^{-1}), micromixing is induced both by the impeller and the impinging jets. Finally, at larger feed flow rates ($Q_t > 5 \times 10^{-3}\,l\,s^{-1}$, or jets velocity higher than $3\,m\,s^{-1}$) the stirring speed has negligible effect showing that micromixing is only controlled by the impinging jets.

When impinging jets are located in position 1 (see Fig. 8) or position 2 (see Fig. 9) the same tendency is observed. However, local energy dissipation rates induced by the impeller are here much lower than in the previous case and even at low feed flow rate micromixing is principally

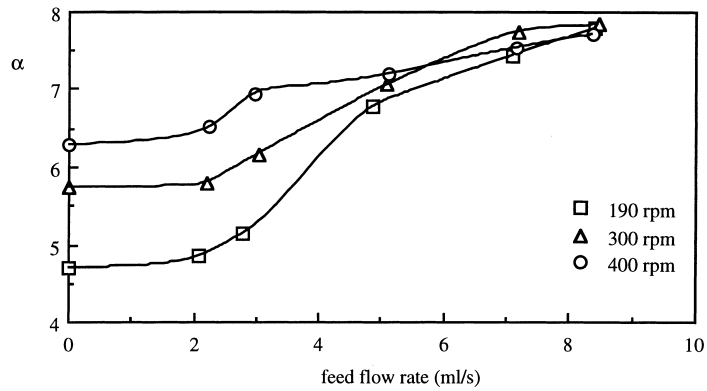

Fig. 7. Evolution of the micromixedness ratio with the total feed flow rate (the impinging jets in location 0).

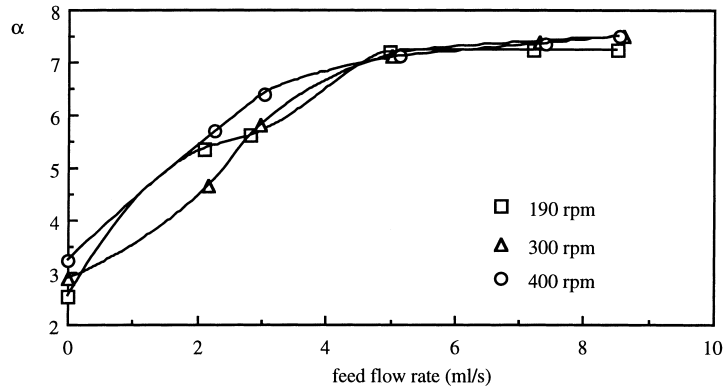

Fig. 8. Evolution of the micromixedness ratio with the total feed flow rate (the impinging jets in location 1).

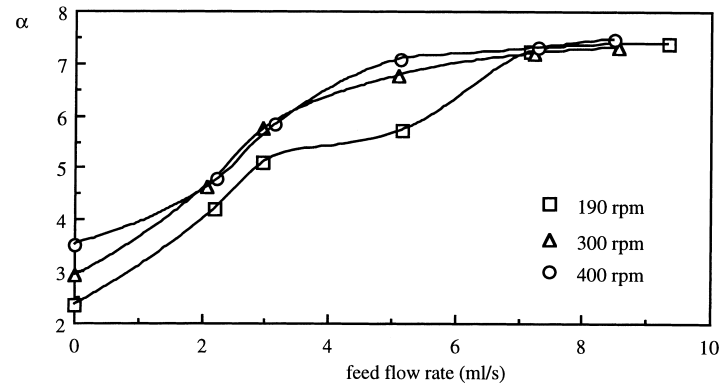

Fig. 9. Evolution of the micromixedness ratio with the total feed flow rate (the impinging jets in location 2).

controlled by the jets. The intermediate domain where the micromixing is induced both by the impinging jets and by the impeller is no more observed. This result shows that even at low feed flow rates, impinging jets are benefit for micromixing.

Furthermore, final values of the micromixedness ratio are almost identical in all cases, whatever the feed position or the stirring speed may be. One can then verify that the impinging jets device prevails over the impeller for large feed flow rates. This can testify to the micromixing efficiency of the impinging jets device toward the simple impeller system.

To verify that impinging jets have a local influence and that they do not disturb the main flow generated by the impeller in the tank, acid was injected far away from the impingement point. As presented in Fig. 10, the feed flow rate has no influence on micromixing efficiency, showing that micromixing is only controlled by the impeller.

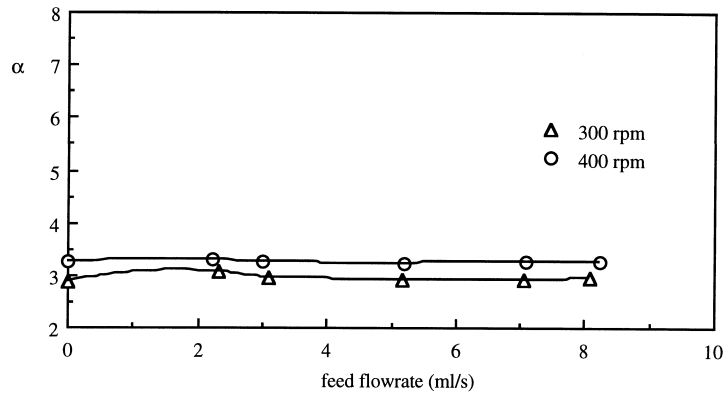

Fig. 10. Evolution of the micromixedness ratio with the total feed flow rate (the impinging jets in location 0, while the sulfuric acid is injected in position 1).

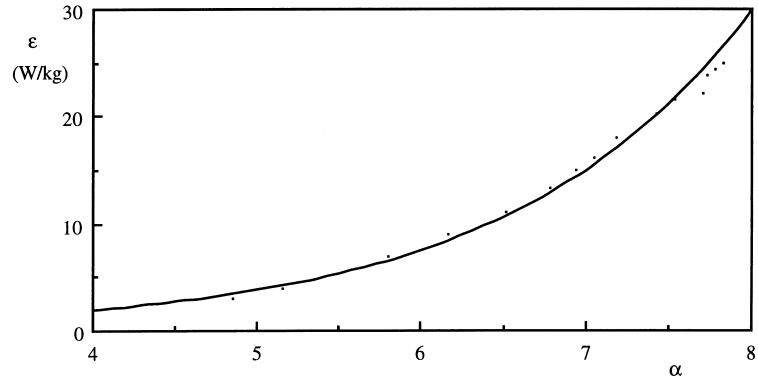

Fig. 11. Local energy dissipation rate as a function of experimental micromixedness ratio for our experimental conditions.

It has been shown that impinging jets have a local influence, and can achieve an increase in micromixing efficiency for large enough feed flow rates.

6. Estimation of the local energy dissipation rates

Local energy dissipation rates are first obtained from chemical test measurements, using a simple micromixing model and the turbulence theory. For impinging jets, the measured local energy dissipation rates are then compared with those obtained from computed fluid dynamics.

6.1. Estimation from chemical test measurements

Using a micromixing model, i.e. the incorporation model, it is possible to estimate micromixing times in the impinging jets. Local energy dissipation rates can then be deduced from the micromixing times, using the turbulence theory.

6.1.1. The incorporation model and the turbulence theory

The incorporation model is derived from earlier works of Villermaux [18] and Villermaux et al. [19], and is clearly described by Fournier et al. [20].

The incorporation model supposes that the fresh acid is divided into aggregates which are progressively invaded by the surrounding fluid, containing iodide, iodate and borate ions. The reactions (i)–(iii) occur in the growing acid aggregates, where mixing is supposed to be achieved. The growing law of the acid aggregates is a function of a characteristic incorporation time t_m, assumed to be the micromixing time. The volume V of an aggregate grows according to the incorporation function

$$V(t) = V_0 \exp\left(\frac{t}{t_m}\right) \tag{11}$$

where V_0 is the volume at initial condition.

For each set of experimental conditions it is possible to calculate the theoretical value of α against the incorporation time by solving the mass balance equations in the aggregates (see Eqs. (7)–(25) in [20]). By equalizing calculated and experimental micromixedness ratios, we can then determine the micromixing time corresponding to the experimental conditions.

According to the Kolmogorov turbulence theory, the micromixing time is proportional to $(\nu/\varepsilon)^{1/2}$, where ε is the local energy dissipation rate, and ν the fluid kinematic viscosity. This variation has been quantified by Baldyga and Bourne [21], who proposed

$$t_m = 17,24\left(\frac{\nu}{\varepsilon}\right)^{1/2} \tag{12}$$

The experimental value of the micromixedness ratio α is then, through the incorporation model, a function of micromixing time t_m and, through relation (12), a function of the local energy dissipation rate ε. For each experimental value of α, it is then possible to deduce the calculated value of t_m, and from t_m the value of ε. Fig. 11 illustrates the dependency of ε versus α for the set of used concentrations.

Turbulent flow generated by the impeller and the impinging jets both contribute to the global dissipation ε. However, we have seen previously, in Figs. 7–10, that the contribution of each device may be highly different in magnitude. Let us estimate their relative contribution.

6.1.2. Local energy dissipation rate of the impeller

Using the method presented above, the local energy dissipation rates of the impeller (for different locations in the reactor) are deduced from the experimental values of α for the experiments performed with no feed flow from the impinging jets.

These results may be compared with data given by different authors (see Table 1), who evaluated, in the same operating conditions (impeller, stirring speed, fluid), the

Table 1
Values of ϕ

Reference	Injection point 0	Injection point 1	Injection point 2
This work	26	0.8	1
Franke and Mersmann [6]	10	1	1
Yu [22]	7.2	0.53	0.88

proportionality constant ϕ defined by

$$\phi = \frac{\varepsilon_{\text{impeller}}}{\bar{\varepsilon}} \tag{13}$$

where $\bar{\varepsilon}$ is the average energy dissipation rate

$$\bar{\varepsilon} = N_{\text{p}} \frac{N^3 D^5}{V} \tag{14}$$

The power number N_{p} in our reactor has been experimentally measured, and found equal to 5.5 for stirring speeds larger than 100 rpm.

The results are presented in Table 1, comparing the experimental values of ϕ for different feeding positions with the values reported by different authors.

The difference between our measured values and the literature data for the injection point 0 is surely derived from the presence of the impinging jets in the reactor, which may disturb the fluid flow around the device. For the two other injection points, the measured values are in good agreements with the reported ones. Subsequently, the measured values of the local energy dissipation rates of the impeller will be compared to the local energy dissipation rates in impinging jets.

6.1.3. Local energy dissipation rates in impinging jets

The local energy dissipation rates of the two mixing devices (impeller and impinging jets) is experimentally deduced from the values of α, according to the incorporation model and relation (12), for different feed flow rates. Indeed, the micromixedness ratio obtained at the impingement point depends on the impinging jets, but also on the agitation. It is not possible to separate the influence of the impinging jets from that of the impeller.

Nevertheless, Figs. 7–9 which indicate that micromixedness ratio is independent of the stirrer speed and the feed position for large feed flow rates, allow to conclude that the local energy dissipation rates thus measured are essentially due to the feeding system.

When impinging jets are in the discharge stream of the impeller, the values of the local energy dissipation rate of the system 'impeller and impinging jets' deduced from the incorporation model and relation (12) evolve alike the measured values of the micromixedness ratio (see Figs. 7 and 12). Three functioning regimes are observed, depending on the feed flow rate. The local energy dissipation rate depends on the stirring speed for small feed flow rate values. It depends on the stirring speed and the feed flow rate at intermediate values, and reaches final values as high as 20 W kg^{-1}, for large feed flow rates: it is no more function of the stirring speed. It is then rather difficult to separate the influence of the impeller from the influence of the impinging jets, especially in the case of low and intermediate feed flow rate values.

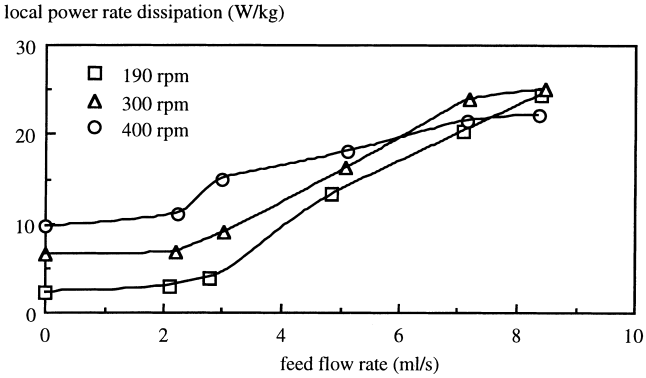

Fig. 12. Local power dissipated by the impinging jets and the impeller against the total feed flow rate (the impinging jets in location 0).

However, when impinging jets are situated in position 1 (Fig. 13) or in position 2 (Fig. 14), the local energy dissipation rate of the impeller is far smaller (see the values corresponding at a zero feed flow rate on Figs. 13 and 14) and the measured values of the energy dissipation rates at the impingement point are therefore mainly owed to the impinging jets. These values, which no more depend on the stirring speed correspond then to the local energy dissipation rate in impinging jets alone. The values of the local energy dissipation rate in impinging jets are then obtained from the experiments performed with feed point position above or below the impeller.

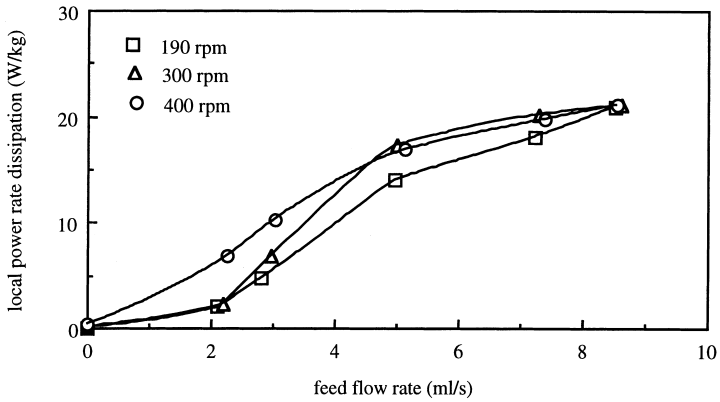

Fig. 13. Local power dissipated by the impinging jets and the impeller against the total feed flow rate (the impinging jets in location 1).

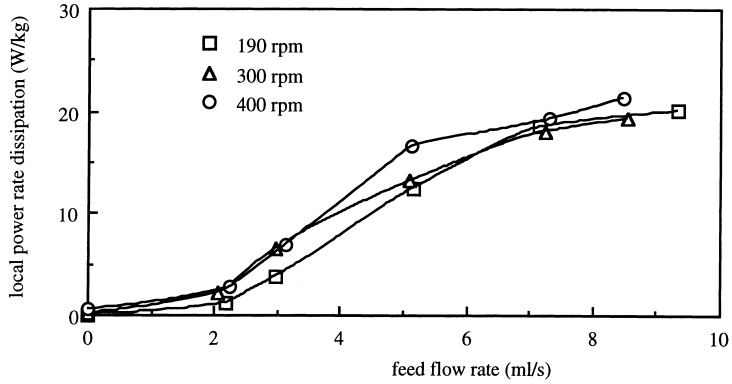

Fig. 14. Local power dissipated by the impinging jets and the impeller against the total feed flow rate (the impinging jets in location 2).

From the experimental data it can be observed that, when the impinging jets are located in position 1 or 2, the additive rule for the energy dissipation rates is valid

$$\varepsilon = \varepsilon_{\text{impinging jets}} + \varepsilon_{\text{impeller}} \tag{15}$$

6.2. Calculation of local energy dissipation rates in impinging jets

Two methods of calculation have been used to estimate the energy dissipation rates: a detailed method based on the resolution of the turbulent flow field using a CFD code and a simple method based on the integrated momentum balance.

6.2.1. Energy dissipation rate estimation from computational fluid dynamics

The computational flow package PHOENICS was used for resolving the continuity equation, the two momentum equations (as the system is axisymmetric) and the equations for the turbulent quantities. We used the low Reynolds turbulent k–ε model from Lam and Bremhorst where k is the turbulent kinetic energy and ε the turbulent energy dissipation rate.

According to the experimental results presented above, we assumed that the turbulent flow in the vicinity of the impinging jets was not influenced by the turbulent flow generated by the impeller. In this case, the calculation domain only considered a small control volume around the jets, avoiding the complex simulation of the whole turbulent flow field in the tank. This assumption is only valid when the jets are placed in position 1 or 2. The zero feed flow rate case has also not been considered. The comparison between experimental and CFD results will then only be performed in these operating conditions.

The calculation results show that in the vicinity of the impingement plane the axial velocity profile is deformed due to the hydrodynamic interaction of the counter current streams and a radial velocity component appears. A disk (thickness δ and radius R) is then generated by impingement of the jets, in the impingement plane (see Fig. 15).

Figs. 16 and 17 present the maximum radial evolution of the velocity and the energy dissipation rate from the impingement point. It can be seen that at the impingement point, the energy dissipation rate can reach very high values of several hundred W kg^{-1}. The radial evolution of ε decays however very strongly with the radial position leading in fact to a much lower average value in volume. To estimate the mean value of the energy dissipation rate we need to know the volume in which micromixing and reactions occur.

According to the incorporation model, the acid aggregates are convected by the turbulent flow up to the total consumption of acid. From the integration of the mass balance in the aggregates (see Eqs. (7) to (25) in [20]), it is possible to determine the time t_{cons} at which the aggregates are totally consumed. As the aggregates are different in size t_{cons} is the consuming time of the mean aggregate size of the whole population. From the velocity field, calculated by CFD, the average radial position R at which the aggregates are consumed can be estimated from

$$t_{\text{cons}} = \int_0^R \frac{dr}{\bar{u}(r)} \tag{16}$$

where $\bar{u}$ is the mean value integrated over the thickness δ of the axisymmetric flow generated by impingement (see Fig. 15).

From the experimental data and the CFD calculation results the order of magnitude of R is around 2×10^{-2} m.

The mean energy dissipation rate is then the mean value integrated on the reaction volume

$$\varepsilon_{\text{jets}} = \frac{\int\int\int \varepsilon(r,z)dv}{\int\int\int dv} \tag{17}$$

with

$$dv = 2\pi\delta r dr \tag{18}$$

The values of ε estimated from CFD calculations are reported in Fig. 18 and compared with values obtained from chemical test measurements. The calculated data are in

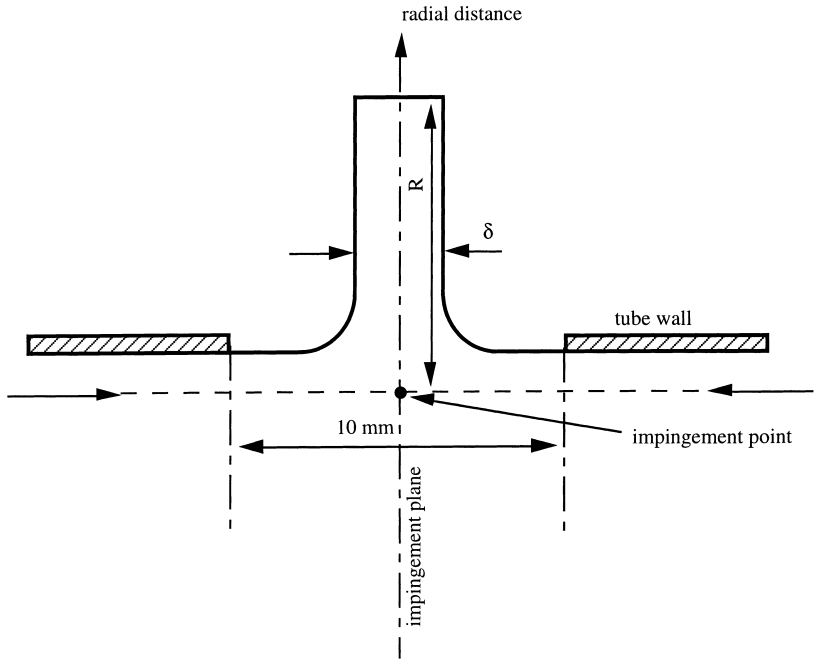

Fig. 15. Sketch of the impinging jet.

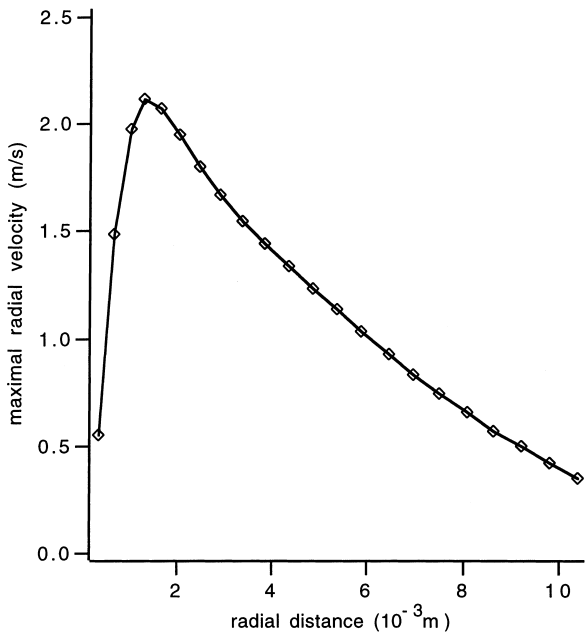

Fig. 16. Evolution of the maximal radial velocity along the radial distance from the impingement point ($Q_t = 5 \times 10^{-3}\,l\,s^{-1}$).

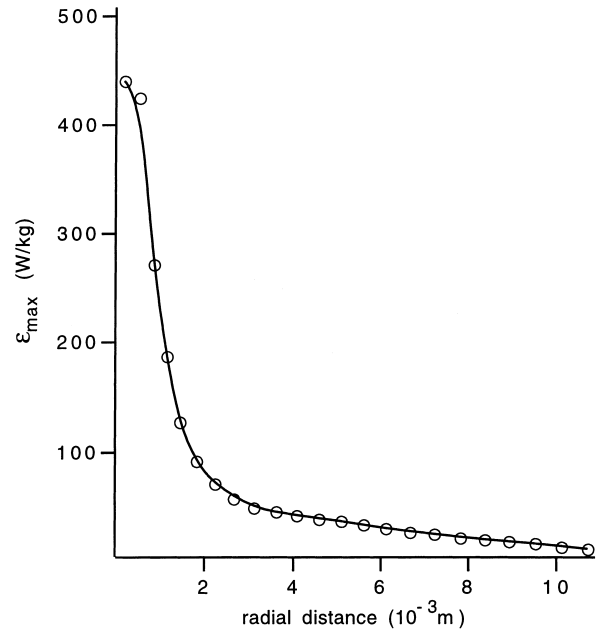

Fig. 17. Evolution of the maximal energy dissipation rate along the radial distance from the impingement point ($Q_t = 5 \times 10^{-3}\,l\,s^{-1}$).

relative good agreement with experiments, but over estimated for high velocity and under estimated for low velocity conditions. Several reasons may be given to explain these discrepancies as the validity of the turbulence model or the validity of the assumptions of the calculations. Nevertheless, we have also to consider the nature of the relation between the micromixedness ratio α and the energy dissipation rate ε. In Fig. 11, it can be seen that the energy dissipation rate has not a great influence on α as α is proportional to $(\varepsilon)^{0.2}$. This means that when the value of ε is multiplied by a factor 2, the difference between the values of α is only 14%. In this sense, we can then say that the calculated data are in relative good agreement with the experimental ones.

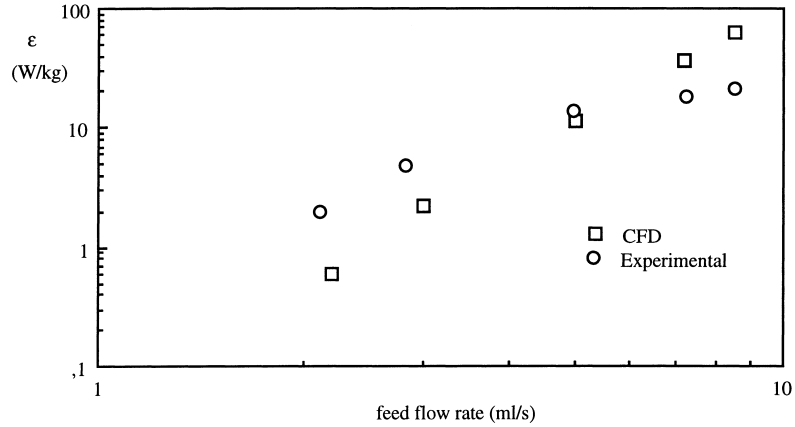

Fig. 18. Variation of the values of ε estimated from CFD and obtained from chemical test measurements against the total feed flow rate.

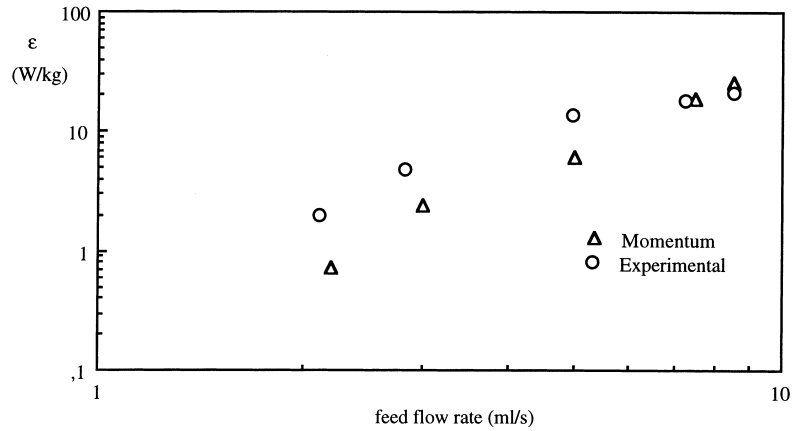

Fig. 19. Variation of the values of ε estimated from momentum balance and obtained from chemical test measurements against the total feed flow rate.

6.2.2. *Energy dissipation rate estimation from simple momentum balance*

The energy dissipation rate can be estimated from the integrated momentum balance on the dissipation volume by

$$\varepsilon_{\text{jet}} = \frac{\left(\frac{1}{2}\rho\bar{u}_{\text{in}}^2 Q_{\text{t}}\right) - \left(\frac{1}{2}\rho\bar{u}_{\text{out}}^2 Q_{\text{t}}\right)}{\int\int\int \rho\, dv} \tag{19}$$

where $\bar{u}_{\text{in}}$ is the mean velocity at the entering zone of the jets, i. e. the tube outlets and $\bar{u}_{\text{out}}$ is the mean velocity in the axisymmetric flow generated by impingement at $r = R$.

In relation (19) the volume of dissipation is calculated from relation (18). The method needs then some calculation results from CFD, as the volume V and the velocities $\bar{u}_{\text{in}}$ and $\bar{u}_{\text{out}}$. The values of ε estimated from Momentum balance are reported in Fig. 19 and compared with values obtained from chemical test measurements. Considering the previous remark on the relation between the micromixedness ratio and the energy dissipation rate, we can say that the calculated data are in relative good agreement with the experimental ones.

6.3. *Micromixing times in impinging jets*

Finally, the values of the micromixing time t_{m} achieved in the device can also be compared.

The 'Experimental' (see Fig. 20) values of t_{m} are deduced from the measured values of α, using the incorporation model. The calculated values of the micromixing time ('CFD' and 'Momentum' in Fig. 20) are deduced from the calculated (Section 6.2) values of ε, according to relation (12). These different values of t_{m} are then compared in Fig. 20. Considering relation (12), which states that the micromixing time varies as the square root of the energy dissipation rate, a slightly better fit is obtained between calculated and experimental values.

Furthermore the order of magnitude of the values of the micromixing time achieved in impinging jets show that the mixing device based on impinging jets is an appropriate and a very simple device for the rapid mixing of two reactants.

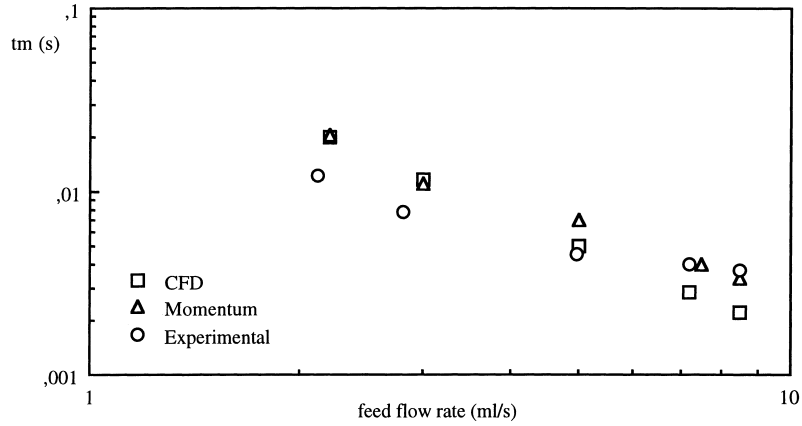

Fig. 20. Calculated and measured values of the micromixing time in impinging jets against the total feed flow rate.

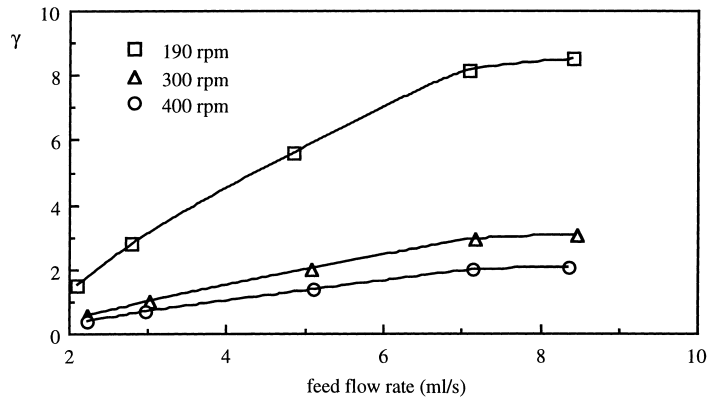

Fig. 21. Evolution of the ratio γ against the total feed flow rate (the impinging jets in location 0).

For example, micromixing times as low as 4 ms are attained for total feed flow rate higher than 8 ml s^{-1}.

6.4. Comparison of local energy dissipation rates at the impingement point

According to the previous results, it can be seen that, at the impingement point, mixing can be completed by the impeller and/or by the impinging jets. At that impingement point, we can therefore compare the values of the power dissipated by these two devices, defining the ratio γ

$$\gamma = \frac{\varepsilon_{\text{impinging jets}}}{\varepsilon_{\text{impeller}}} \tag{20}$$

The local energy dissipation rates are here obtained from the performed chemical test measurements. The values of $\varepsilon_{\text{impeller}}$ are deduced from experiments performed at null feed flow rate, whereas those of $\varepsilon_{\text{impinging jets}}$ are deduced from relation (15) for experiments performed in position 1 and 2.

In the discharge stream of the impeller (position 0), the ratio γ is calculated according to the values of $\varepsilon_{\text{impinging jets}}$ obtained in position 1, and according to the experimental value of $\varepsilon_{\text{impeller}}$. The choice of the literature data for the value of $\varepsilon_{\text{impeller}}$ would not change drastically the order of magnitude of γ in position 0 and the results would have lead to the same conclusion.

In the discharge stream of the impeller (position 0, Fig. 21), it can be seen that the local energy dissipation rate in impinging jets is of the same order of that locally dissipated by the impeller. For stirring speeds of 300 or 400 rpm, the ratio γ remains smaller than 3, even at large feed flow rates. For smaller stirring speeds, γ can reach values as high as 8, which is significant of a clear prevalence of the impinging jets over the impeller.

When impinging jets are situated in position 1 (Fig. 22) or in position 2 (Fig. 23), the ratio γ can reach values higher than 100. In this case, impinging jets dissipate powers largely superior to that dissipated locally by the impeller.

Impinging jets achieve then a very good initial micromixing between fresh reactants, dissipating locally powers far higher as those of the impeller and leading to micromixing times, for large feed flow rates, as small as 4 ms (Section 6.2). This high level of energy dissipation rates presents two great advantages:

1. On one hand, as good micromixing conditions can be achieved, high and particularly reproductive initial supersaturation levels can be obtained, which can result

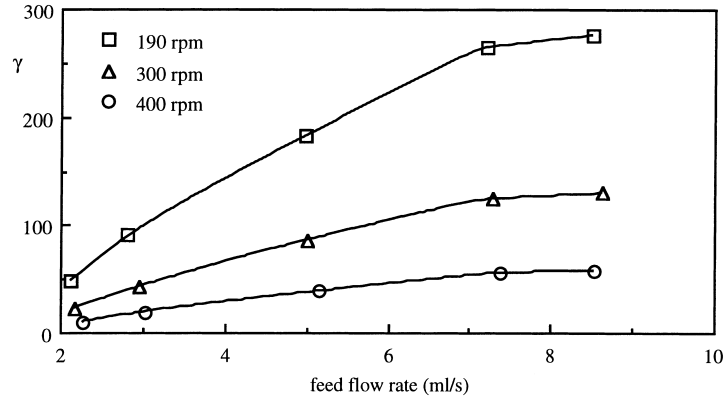

Fig. 22. Evolution of the ratio γ against the total feed flow rate (the impinging jets in location 1).

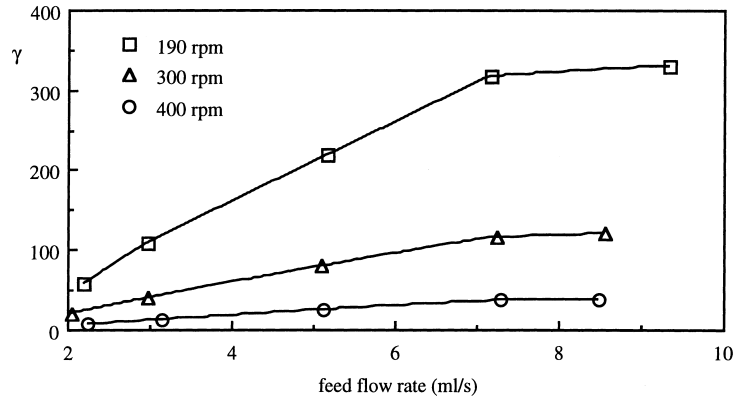

Fig. 23. Evolution of the ratio γ against the total feed flow rate (the impinging jets in location 2).

in the production of a precipitate fulfilling very specific qualities and reproductive characteristics.

2. On the other hand, as the ratio of the local energy dissipation rates at the impingement point can be quantified, a process using impinging jets could easily be extrapolated at higher scale, conserving, for example, the values of the power dissipated by the impeller and the impinging jets at the impingement point. Knowing that the local energy dissipation rate is proportional to the second power of the jet velocity, we recommend, as a first approximation, to keep constant the jet velocity for the scale up.

7. Conclusion

A chemical system of parallel competing reactions based on the Dushman's reaction is successfully used to determine the micromixing quality of an impinging jets device placed in different positions in a stirred tank. Interesting results are obtained comparing the influence of the impinging jets to the influence of the stirrer on micromixing at the impingement point. Three operating zones can be distinguished from these results. For jet velocities lower than 2 m s^{-1}, the influence of the impinging jets on the micromixing level is insignificant, while for jet velocities higher than 5 m s^{-1} the mixing action of impinging jets is not disturbed by the stirrer. Jet velocities between 2 and 5 m s^{-1} delimit an intermediate zone where the influence of the impinging jets and the influence of the stirrer on the micromixing level are comparable to each other.

Micromixing times calculated from the experimental data show that the mixing device based on impinging jets is an appropriate and a very simple device for rapid mixing of reactants. For example, micromixing times as low as 4 ms are obtained for jet velocities higher than 5 m s^{-1}.

The energy dissipation rate at the impingement point is deduced from our experiments using the incorporation model and the turbulence theory. The corresponding values show that the impinging jets can realise a high local dissipation rate. For example, values greater than 20 W kg^{-1} are obtained for jet velocities higher than 5 m s^{-1}. At the same time, the energy dissipation rates calculated by a CFD-package (Phoenics) are in good agreement with experimental data. The ratio of power dissipated by the impinging jets to that dissipated by the stirrer can vary in a large interval depending on the jet velocity and the impingement position in the tank. Values of this ratio as high as 100 can be obtained for jet velocities higher than 5 m s^{-1} and for several chosen positions.

The mixing action of the impinging jets is concentrated in a very small volume of the stirred tank where the energy

dissipation rate can reach very high values. Thus, for many rapid processes (for example, precipitation and polymerization) requiring a vigorous mixing during the initial contact of the reactants, the use of the impinging jets device represents an attractive solution. In this case, the stirrer can supply moderate power to the whole volume of the tank, while the impinging jets concentrate high power values there where they are needed. In addition, the scale up of this device is easy to realise keeping constant the jet velocity.

8. Notation

C_j	concentration of reactant j (mol m^{-3})
D	impeller diameter (m)
D_{353}	optical density at 353 nm
d	thickness of quartz cell (m)
K	equilibrium constant of the reaction (iii) (m^3 mol^{-1})
N	stirring speed (s^{-1})
N_p	power number
n_j	quantity of reactant j (mol)
Q_t	total feed flow rate of the jets (m^3 s^{-1} or ml s^{-1})
Re	Reynolds number
R	radial position at which the aggregates are totally consumed (m)
T	vessel diameter (m)
t	time (s)
t_c	minimum time beyond which the segregation index value remains constant (s)
t_{cons}	time at which the aggregates are totally consumed (s)
t_m	physical micromixing time (s)
t_r	chemical reaction time of the reaction (ii) (s)
u	jet radial velocity (m s^{-1})
V	liquid volume in the vessel (m^3)
$V(t)$	volume of acid aggregates (m^3)
X	extent of reaction
X_s	segregation index
Y	yield of the reaction (ii)

Greek letters

α	micromixedness ratio
γ	ratio relating impinging jets and impeller local energy dissipation rate
δ	thickness of the axisymmetric flow generated by impingement (m)
$\varepsilon_{I_3^-}$	molar extinction coefficient of triiodide ions (mol^{-1} m^2)
ε	local energy dissipation rate (W kg^{-1})
ϕ	proportionality constant relating average and local energy dissipation rates
ν	fluid kinematic viscosity (m^2 s^{-1})
ρ	density (kg m^{-3})

Subscripts

PM	Perfect Mixing conditions
TS	Total Segregation conditions
tot	total
1	reaction (i)
2	reaction (ii)

Superscripts

0	initial
–	average

References

[1] J. Garside, N.S. Tavare, Chem. Eng. Sci. 40 (1985) 1485.
[2] B. Marcant, R. David, AIChE J. 37 (1991) 1698.
[3] R. David, B. Marcant, AIChE J. 40 (1994) 424.
[4] A. Mersmann, M. Kind, Chem. Eng. Technol. 40 (1988) 264.
[5] B.L. Aslund, A.C. Rasmuson, AIChE J. 38 (1992) 328.
[6] J. Franke, A. Mersmann, Chem. Eng. Sci. 50(11) (1995) 1737–1753.
[7] A. Tamir, A. Kitron, Chem. Eng. Commun. 50 (1987) 241.
[8] M. Midler, E.L. Paul, E.F. Whittington, Engineering Foundation Conference on Mixing, Potosi, MO. Production of high purity, high surface area crystalline solids by turbulent contacting and controlled secondary nucleation, 1989.
[9] P.D. Liu, M. Futran, M. Midler, E.L. Paul, AIChE Meeting, Chicago, Particle size design of pharmaceuticals by continuously impinging jets precipitation, 1990.
[10] A.J. Mahajan, D.J. Kirwan, AIChE J. 42(7) (1996) 1801–1814.
[11] J.R. Bourne, Chem. Eng. Commun. 16 (1982) 79.
[12] M.C. Fournier, Ph-D Thesis, Institut National Polytechnique de Lorraine, Nancy, 1994.
[13] P. Guichardon, Ph-D Thesis, Institut National Polytechnique de Lorraine, Nancy, 1996.
[14] D.A. Palmer, M.H. Lietzke, Radiochimica Acta 31 (1982) 37–44.
[15] J. Villermaux, Micromixing phenomena in stirred reactors in Encyclopedia of Fluid Mechanics, Gulf Publishing Company, 1986, pp. 707–771.
[16] F.A. Holland, F.S. Chapman, Liquid mixing and processing in stirred tanks, Reinhold Publishing, New York, 1966.
[17] J.R. Bourne, S.A. Thoma, Trans. Instn. Chem. Engrs. A. 69 (1991) 321–323.
[18] J. Villermaux, AIChE Meeting, Chicago, Paper 185a, Micromixing and chemical reaction: semi-quantitative criteria based on comparison of characteristic time constants, 1990.
[19] J. Villermaux, L. Falk, M.C. Fournier, AIChE Symp. Ser. 286(88) (1992) 6–10.
[20] M.C. Fournier, L. Falk, J. Villermaux, Chem. Eng. Sci. 51(23) (1996) 5187–5192.
[21] J. Baldyga, J.R. Bourne, Chem. Eng. J. 45 (1990) 25–31.
[22] S. Yu, Ph-D Thesis, Swiss Federal Institute of Technology, Zürich, 1993.
[23] M.C. Fournier, L. Falk, J. Villermaux, Chem. Eng. Sci 51(22) (1996) 5053–5064.